# Wind Tunnel Based System Identification of a Small Unmanned Aircraft System

Sabine Wisbacher * and Daniel Ossmann†
*Munich University of Applied Sciences HM, 80335 Munich, Germany*

Sebastian Schubert‡, Jürgen Frey§ and Harald Pfifer ¶
*Technische Universität Dresden, 01307 Dresden, Germany*

**This paper presents the setup and results of a wind tunnel test campaign conducted to identify and analyze the short period dynamics of a small unmanned aircraft system. The experiments are performed in the Göttingen-type wind tunnel operated by the Chair of Flight Mechanics at the TU Dresden. A specially designed test rig enables static and dynamic testing with the aircraft being either fixed or having a pitching degree of freedom. In the static test campaign time averaged data collected with a six component balance is used to determine the static aerodynamic derivatives. Additionally, the aircraft's pitching dynamics, including pitch damping are investigated with the dynamic test configuration. With a *grey box* identification approach parameters characterizing these dynamics are estimated from pitch rate data collected with a Pixhawk 6x. By combining static and dynamic test results, a complete parameter set for linear short period models is obtained. Analysis of the models' natural frequency and damping ratio across the airspeed range demonstrates behavior consistent with realistic short period dynamics. This altogether strengthens the confidence in the ability of the test setup to provide an efficient, safe and easy way to gain insight in the short period dynamics of small unmanned aircraft systems.**

## I. Introduction

The application range of Unmanned Aircraft Systems (UAS) is rapidly evolving. Especially fixed-wing UAS with their ability to carry bigger payloads over long distances are used within a variety of fields such as aerial mapping, inspection of suppliance lines as well as public security. In each of those applications a successful execution of the mission depends heavily on the control design implemented on the flight computer. Those control strategies are usually developed using linear models to predict the UAS behavior and determine control parameters. A linear mathematical representation of the aircraft behavior is thus essential for the development of advanced flight control and path optimization.

There are various ways to obtain a mathematical representation. A common way of getting models is via system identification from flight test data. For example in [1] a parametric *grey box* approach is used to determine accurate nonlinear dynamic models for a small fixed-wing UAS. And in [2] *grey box* as well as *black box* methods are used for the identification of linear models for a UAS with flexible wings. A comprehensive overview of the different approaches is given in [3] and a more detailed list of their application for the identification of UAS in literature can be found in [4].

Flight tests however can only be done at a rather final stage of aircraft development and already require some knowledge on the limitations of the aircraft. Additionally in any flight test scenario measurement errors, unmeasured disturbances and changing flight conditions influence the quality of the gathered data. While measurement errors are an inevitable part of every experimental setup, the problems of unmeasured disturbances and changing flight conditions can be solved by moving the experiment to a wind tunnel. This approach is called dynamic wind tunnel testing and is especially useful for UAS as they are oftentimes small enough to be tested within a wind tunnel at full scale. A key benefit of the dynamic wind tunnel testing is the fact that the aircraft is attached within the track of the wind tunnel. This has been used in [5] to collect additional information such as aerodynamic load and angle measurements from the

*Research Assistant, Department of Mechanical, Automotive and Aeronautical Engineering, sabine.wisbacher@hm.edu
†Professor, Department of Mechanical, Automotive and Aeronautical Engineering, daniel.ossmann@hm.edu, AIAA Senior Member
‡Research Assistant, Chair of Flight Mechanics and Control, sebastian.schubert@tu-dresden.de
§Research Assistant, Chair of Flight Mechanics and Control, juergen.frey@tu-dresden.de
¶Professor, Chair of Flight Mechanics and Control, harald.pfifer@tu-dresden.de

experiment. In [6] and [7] the test rig serves as risk mitigation to allow the investigation of dynamics at the edge of the flight envelope without the risk of loosing the vehicle. However, careful consideration must be given to the experimental design to ensure that the investigated dynamics are captured accurately. Various strategies have been developed to tackle that challenge. For instance, in [8], a test rig with varying degrees of freedom is used to isolate and investigate different dynamic aspects individually. And a combination of static and dynamic tests, using forced oscillations, is applied in [9] to identify aerodynamic derivatives for a small delta wing UAS. For a more comprehensive overview of the available testing techniques, the reader is referred to [10] and [11]. In general, dynamic wind tunnel testing has proven to provide valuable insights into aircraft dynamics, offering a safer and more controllable alternative to flight testing.

In this paper a wind tunnel test campaign including both static and dynamic tests with a pitching degree of freedom is conducted in order to investigate the short period dynamics of a small fixed wing UAS under varying flight conditions. The results from both experiments are used to determine parameters for building a linear short period model, as outlined in Section II. The tests are performed at the Göttingen-type wind tunnel operated by the Chair of Flight Mechanics at TU Dresden, using a specially designed test rig. The experimental design, along with a description of the test rig, is provided in Section III. The resulting models are evaluated in Section IV by analyzing and comparing their natural frequency and damping ratio across all investigated flight conditions.

## II. Fundamentals

System identification as a part of system theory deals with the mathematical modeling to gain insight into system dynamics [12]. This process is essential for applications such as experiment designs, predicting system behavior and controller design. There are various types of models that can be used as mathematical representations of the system behavior ranging from *white box* models based on physical laws with corresponding parameters and *grey box* models with adjustable parameters to subspace based *black box* models [12]. Choosing those candidate models is one of three entities that build the identification procedure. The choice generally depends on factors like prior knowledge of the system dynamics, available test equipment (i.e. obtainable data) and requirements of the model. Another entity of the identification process is the recording of data, which consists of the experimental design, including the choice of input signals and recorded data. As the availability of test equipment influences the choice of model structure and the model structure determines the experiment design, those entities are closely connected. In this work, the parameters defining the short-period dynamics of the Urban Condor are identified using both *white box* and *grey box* methods.

### A. System Identification

In the *white box* identification approach, parameters are measured directly. In contrast, for the *grey-box* approach, a model is defined based on the parameter vector $\theta$, and its response to an input is compared to the observed real dynamic behavior of the system. The structure of the parameterized model can vary and may include nonlinear models. In this work however a state space structure

$$\begin{aligned} \dot{x}(t) &= A(\theta)x(t) + B(\theta)u(t) \\ y(t) &= C(\theta)x(t) + D(\theta)u(t) \end{aligned} \tag{1}$$

with the states $x \in \mathbb{R}^n$, the input vector $u \in \mathbb{R}^p$, the output vector $y \in \mathbb{R}^q$ and the state space matrices $A \in \mathbb{R}^{n\times n}$, $B \in \mathbb{R}^{n\times p}$, $C \in \mathbb{R}^{q\times n}$, and $D \in \mathbb{R}^{q\times p}$ is used. The parameters of the defined model are adjusted iteratively to minimize the error between the measured data and the predicted model response [3]. This leads to an optimization problem targeting the so-called prediction error

$$e(t_i, \theta) = y(t_i) - \hat{y}(t_i, \theta) \tag{2}$$

between the measured data $y(k)$ and the prediction $\hat{y}(k, \theta)$ at the time instance $t_i$ based on the parameterized model [13]. The quality of the model is thus judged by its ability to predict the real-world behavior of the system. In general, a model is good if the prediction error is small. There are however different ways to specify what a small prediction error means [13]. In this work the quadratic norm

$$||e(\theta)||_2 = \frac{1}{N}\sum_{i=1}^{N}\frac{1}{2}e(t_i, \theta)^T e(t_i, \theta) \tag{3}$$

refering to the size of the error $e$ over the scope of an experiment with $N$ data points is used. To find the parameter vector leading to the smallest prediction error an optimization problem is solved based on an initial guess with the

optimal parameter being defined as [13]:

$$\hat{\theta} = \arg\min_{\theta} ||e(\theta)||_2 \tag{4}$$

There are different least squares search methods that can be used to solve the optimization problem, such as a subspace Gauss-Newton, Levenberg-Marquardt and steepest descent least-squares search. The methods are described in more detail in [3]. In general all of those methods can only find local minima and are thus highly dependent on a good initial guess for the parameter vector $\theta$ [2]. In this work the MATLAB System Identification Toolbox is used. With the Toolbox different search methods are tested in each iteration and the first search result that leads to a reduction of cost is used.

### B. Parametric Short Period Model

The short period motion is a fast responding longitudinal mode that can be excited from a trimmed flight condition by applying an elevator deflection input $\eta$. The dynamics of the short period motion can generally be represented in a linear form as follows:

$$\begin{bmatrix} \dot{\alpha} \\ \dot{q} \end{bmatrix} = \begin{bmatrix} Z_\alpha & 1 \\ M_\alpha & M_q \end{bmatrix} \begin{bmatrix} \alpha \\ q \end{bmatrix} + \begin{bmatrix} Z_\eta \\ M_\eta \end{bmatrix} \eta \tag{5}$$

where the angle of attack $\alpha$ and the pitch rate $q$ are the states of the motion and $Z_\alpha$, $Z_\eta$, $M_\alpha$, $M_q$, $M_\eta$ are the dimensional aerodynamic derivatives. Specifically, $Z_\alpha$ and $M_\alpha$ describe the effect of a change in the lift force and pitch moment due to variations in the angle of attack. Similarly, $Z_\eta$ and $M_\eta$ represent the effect of a change in the lift force and pitch moment influenced by an elevator deflection. The coefficient $M_q$ captures the effect of a change in the pitch moment due to pitch rate variations. Note that, since the aircraft under consideration has a standard tailplane configuration the effects of pitch rate variations on the overall produced lift force is assumed to be negligible and the corresponding aerodynamic coefficient $Z_q$ is therefore not included in Eq. (5). For the parameterized model the dynamic pressure $\bar{q}$, the wing planform area $S$, the chord length $\bar{c}$, the mass $m$ of the aircraft and its inertia about the pitching axis $I_y$ as well as the absolute flight speed $v_0$ are used to formulate the dimensional coefficients depending on dimensionless derivatives:

$$\begin{aligned} Z_\alpha &= -\frac{\bar{q}S}{mv_0} C_{L\alpha} & & & Z_\eta &= -\frac{\bar{q}S}{mv_0} C_{L\eta} \\ M_\alpha &= \frac{\bar{q}S\bar{c}}{I_y} C_{m\alpha} & M_q &= \frac{\bar{q}S\bar{c}^2}{2I_y v_0} C_{mq} & M_\eta &= \frac{\bar{q}S\bar{c}}{I_y} C_{m\eta} \end{aligned} \tag{6}$$

The dimensionless derivatives $C_{L\alpha}$, $C_{m\alpha}$, $C_{L\eta}$, $C_{m\eta}$ and $C_{mq}$ are independent of the specific flight condition, making them more universally applicable across varying scenarios. From those dimensionless parameters $C_{L\alpha}$ and $C_{L\eta}$ as well as $C_{m\alpha}$ and $C_{m\eta}$ can be determined using *white box* identification methods. These parameters are directly obtained from time averaged data collected in a static wind tunnel test. In contrast, the derivation of $C_{mq}$ requires a dynamic test setup. However, since $C_{L\alpha}$ and $C_{L\eta}$ are already obtained through static testing, the dynamic setup does not need to account for vertical motion. This significantly simplifies the experimental requirements, as a test rig featuring only a pitching degree of freedom is sufficient to replicate the rotational dynamics needed to evaluate the pitch damping $C_{mq}$. The motion of an airplane within such a test rig can be expressed as:

$$\begin{bmatrix} \dot{\Theta} \\ \dot{q} \end{bmatrix} = \begin{bmatrix} 0 & 1 \\ \frac{\bar{q}S\bar{c}}{I_y^*} C_{m\alpha} & \frac{\bar{q}S\bar{c}^2}{2I_y^* v_0} C_{mq} \end{bmatrix} \begin{bmatrix} \Theta \\ q \end{bmatrix} + \begin{bmatrix} 0 \\ \frac{\bar{q}S\bar{c}}{I_y^*} C_{m\eta} \end{bmatrix} \eta \tag{7}$$

where $\Theta$ is the pitch angle of the aircraft. Generally the movement in this dynamic test setup is similar to the rotational dynamics of the short period motion. The key difference is, that the angle of attack is not influenced by translational motion and is thus equal to the pitch angle. Furthermore, any misalignment between the aircraft's center of gravity and the test rig's rotational axis must be taken into account in the inertia $I_y^*$ about the pitching axis of the test rig. Since the derivatives $C_{m\alpha}$, $C_{m\eta}$ and $C_{mq}$ all influence this motion, all three parameters can be determined from the dynamic test using *grey box* identification. This allows for further validation of the identification methods by comparing the results obtained from both static and dynamic tests for $C_{m\alpha}$ and $C_{m\eta}$.

## III. Wind Tunnel Facilities and Experimental Setup

The Chair of Flight Mechanics and Control at TU Dresden operates a low-speed Göttingen-type wind tunnel with a closed circuit but a 4.5 m long open test section, as depicted in Fig. 1. The tunnel has a circular nozzle with a 3-meter

diameter and provides flow velocities of up to 40 m/s. Its contraction ratio is 7:1, leading to a free stream turbulence below 0.5 %, which makes it suitable for conventional aeronautical applications like the system identification presented in this work.

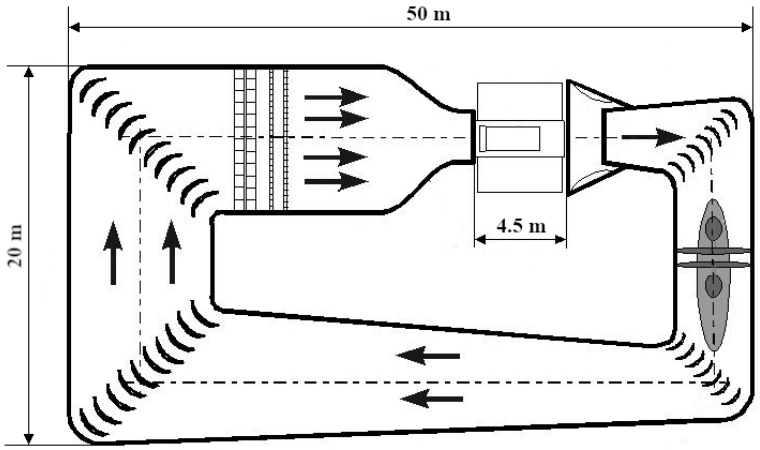


**Fig. 1 Schematic illustration of TU Dresden's wind tunnel.**

The UAS to be identified is the so-called Urban Condor. It is based on a Sig Kadet LT-40 with a modified 3D-printed wing. The new wing has an increased wingspan of 2 m over the conventional LT-40 wing and includes high-lift devices. Its modular design also enables quick repairs and easy adaptation by switching sections, e.g. adding wing sections with different sensor concepts like pressure probes. Urban Condor has an empty weight of 5.5 kg, its cruise speed is about 17 m/s, and the minimum landing speed is approximately 10 m/s. A Pixhawk 6x flight control unit is used to command the elevators during the experiment, as well as record accelerometer, gyroscope and magnetometer data from the internal IMU at a sample rate of 50 Hz. The data is recorded in log files using the Mission Planner interface which also allows the elevator position to be either adapted manually or follow a predefined signal. The aircraft in the wind tunnel setup

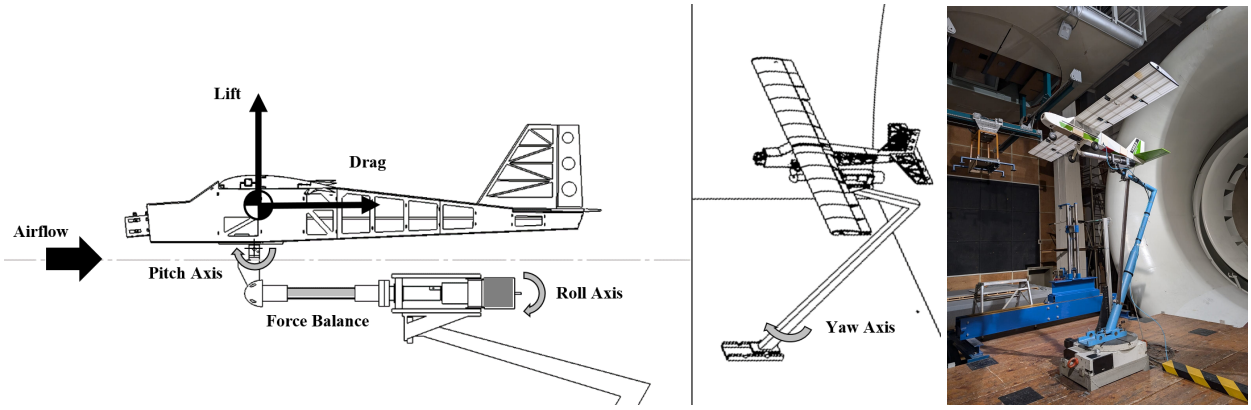


**Fig. 2 UAV Urban Condor mounted on the specially developed test-stand in the wind tunnel.**

is shown in Fig. 2. The UAS is mounted in the test section on a traverse system which allows rolling and yawing the aircraft. In the pitch axis the aircraft is mounted on a low friction pitching joint which can either be fixed or allow the aircraft to pitch during the experiments. This is realized by a machined stainless-steel shaft and a plain bearing sleeve. A six-component force balance is located between the roll and pitch axis of the traverse system. In addition to the three forces and moments acting on the UAV, the free stream velocity is calculated by the wind tunnel measurement system via the free stream dynamic pressure and the temperature. An electronic trigger signal is implemented to synchronize the measurements from the wind tunnel system with those from the Pixhawk. With this flexible setup a combination of static and dynamic wind tunnel tests can be realized that already enables the determination of full short period models.

### A. Static Test Cases

For the static wind tunnel tests the joint is fixed while the traverse system is adjusted to achieve aircraft positions with different angle of attacks within the airflow. All static tests are conducted at an airspeed of 15 m/s. To achieve the angle of attack positions the roll axis of the traverse system is used to place the aircraft with a 90 deg bank angle within the airflow. In this position the yawing axis of the traverse system can be used to adjust the angle of attack. For each angle of attack, time-averaged data is collected from the six-component balance to determine the lift and moment generated by the Urban Condor. Similarly, the lift and moment produced by the UAS are measured for different elevator deflections. These measurements are then repeated across a range of angles of attack to analyze any possible interactions. A summery of the static test cases is given in Table 1

**Table 1 Static wind tunnel test cases**

| Angle of attack (deg) | 0 | ±1 | ±3 | ±5 | ±7 | ±9 | ±10 | ±11 | ±13 | ±15 | ±17 | ±19 | ±20 |
|---|---|---|---|---|---|---|---|---|---|---|---|---|---|
| Elevator deflection (deg) | 0 | 0 | 0 | 0 | 0 | 0 | 0 | 0 | 0 | 0 | 0 | 0 | 0 |
| | ±15 | - | - | ±15 | - | - | ±15 | - | - | - | - | - | - |
| | ±30 | - | - | ±30 | - | - | ±30 | - | - | - | - | - | - |

### B. Dynamic Test Cases

In the dynamic test setup, the roll and yaw axes of the traverse system are fixed at zero, while the pitch joint remains free to allow the aircraft to pitch freely around the joint position. The rotational axis of that pitching motion is in x-direction and y-direction aligned with the centre of gravity of the UAS but has a small offset in z-direction. In contrast to the static setup, the dynamic setup records time series of measurements instead of time-averaged data to capture the aircraft's dynamic response to excitation within the test rig. The pitching motion of the aircraft on the test rig in the dynamic test configuration is excited using predefined elevator deflection signals. To effectively capture the pitching dynamics, these input signals must encompass a broad frequency range, both below and above the estimated natural frequency of the motion [3]. The natural frequency of the pitching motion is estimated to be within the same area but slightly lower than the short period mode since the influence of the vertical movement is omitted. Based on a basic model developed using the Athena Vortex Lattice (AVL) aerodynamics analysis program [14], the short-period frequency for the Urban Condor at its cruise speed of 17 m/s is estimated to be approximately 1.5 Hz. Therefore, to sufficiently excite the pitching dynamics, an appropriate input signal must cover frequencies below and above 1.5 Hz. The input signals which are designed for that, namely two chirps and a 3211 signal, are depicted in the left diagrams of Fig. 3.

The upper left diagram of Fig. 3 shows a chirp signal of the form $\Delta\eta = A_{\text{chirp}} \sin(\omega t)$. To ensure the chirp covers the relevant frequency range the signal starts at a frequency of $\omega = 0.2$ Hz that increases to 2 Hz linearly over the test duration of 20 s. Analyzing the frequency content of the signal in the right diagram of Fig. 3, indicates that the magnitudes of the chirp signal are high in the relevant frequency range and decrease sharply at higher frequencies. This provides a very clear excitation of the frequency range that the natural frequency of the pitching motion is estimated to be in. The second input signal, depicted in the second diagram on the left side of Fig. 3, is also a chirp input. However, as can be seen in the spectrum in the right diagram, the second chirp signal is designed to cover a slightly smaller frequency range compared to the first signal.

In the lower left diagram the third input signal is shown. It is a 3211 signal that is commonly used in flight tests to excite short period dynamics. It consists of four impulses with varying amplitudes directly following each other. The first impulse has a duration of $3\Delta t$, the second $2\Delta t$ followed by two impulses with $\Delta t$. The amplitudes and length of the 3211 signal are adapted as suggested in [3]. The objective is to generate an input spectrum which places the estimated frequency of the pitching mode at the center of its upper third, with the magnitude being spread as equally as possible throughout the spectrum. The time step $\Delta t$ of the 3211 signal is selected based on the estimated natural frequency $\omega_n$ as 0.2 s with $\Delta t \approx 0.3/\omega_n$ to achieve the placement of the short period frequency at the upper third of the input spectrum. The amplitudes are adapted so that the first impulse shows 67 % of the reference amplitude $A_{3211}$, the second impulse shows the full amplitude and the short impulses at the end of the sequence shows 92 % of the reference amplitude. This shifts the frequency spectrum of the 3211 signal to be more equally spread across the relevant frequencies.

To summarize, the frequency spectrum of the 3211 signal has a more equal spread of magnitude along all frequencies,

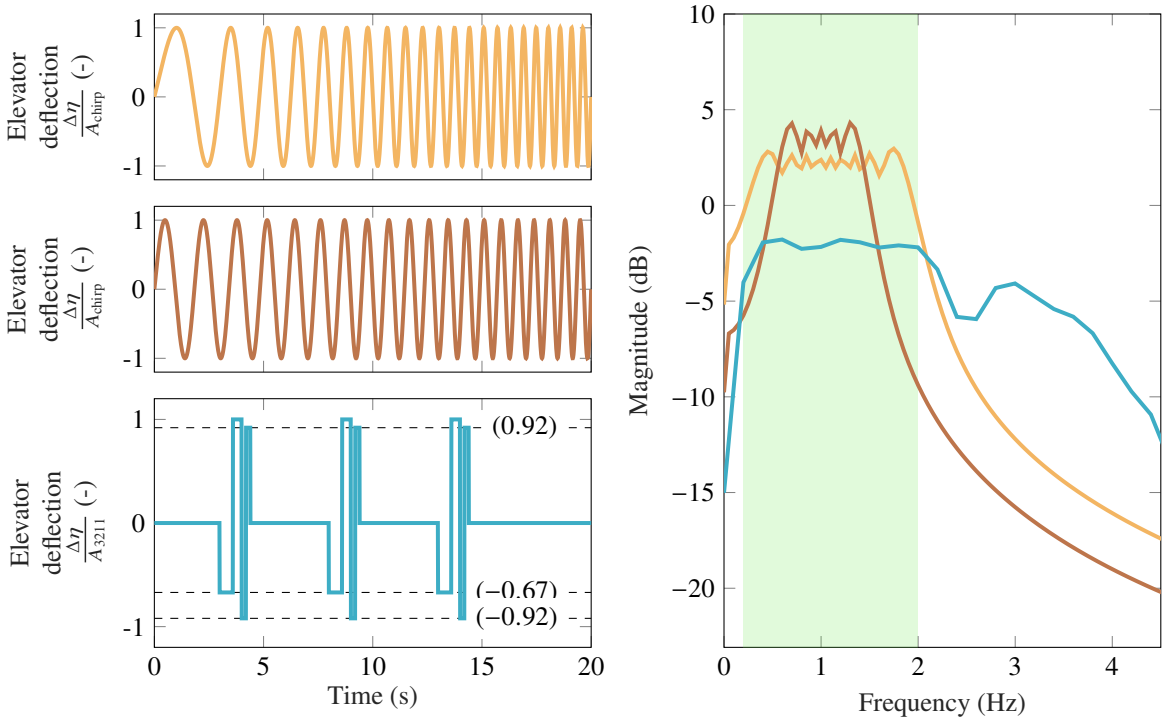


**Fig. 3 Selected types of elevator input signals on the left and their frequency analysis on the right.**

while the chirp signal provides a stronger excitation of the lower frequency spectrum. Within the scope of this work the first chirp input signal is used for the identification test cases as it provides a stronger excitation profile within the relevant frequency range. The second chirp as well as the 3211 input signal is later used to verify the resulting models of the pitching motion by providing independent test data.

For each input signal, experiments are conducted at eleven different airspeeds starting from 15 m/s up to 25 m/s. Testing the vehicle dynamics at a variety of speeds provides valuable insight on how the aircraft dynamics change throughout those conditions. It further enables an in-depth validation of the used identification approach, as problems can be identified more easily when different test scenarios are available. At each tested airspeed the elevator trim point is determined by adapting the elevator input manually until the lift, measured by the six-component scale of the wind tunnel measurement system, is equal to the weight of the LT40 aircraft. The maximum possible elevator deflections around that trim point for both signals are then determined to ensure that the aircraft stays within the limitations of the test rig during the actual test sequences. This information is then used to specify the properties of the chirp as well as the 3211 signals. A detailed overview of the signal attributes is provided in Table 2. At higher airspeed larger elevator deflections are necessary to trim the aircraft due to the backwards pitching moment caused by the increase in wing lift. The main constraint for the elevator deflection is the upper limit due to the test stand construction. Thus, the further the trim value is downwards (positive), the larger the input signal amplitudes can be selected enabling larger excitation and thus, a better signal-to-noise ratio. This trend is clearly given within the defined elevator deflection limits listed in Table 2.

**Table 2 Dynamic wind tunnel test cases**

| Airspeed (m/s) | 15 | 16 | 17 | 18 | 19 | 20 | 21 | 22 | 23 | 24 | 25 |
|---|---|---|---|---|---|---|---|---|---|---|---|
| elevator trim value $\eta_{\text{trim}}$ (deg) | 2 | 3.2 | 4.1 | 5 | 5.2 | 5.8 | 6.1 | 6.4 | 6.5 | 6.8 | 7 |
| input signal amplitude $A_{\text{chirp}}/A_{3211}$ (deg) | 8 | 11 | 12 | 13 | 14 | 14.2 | 14.5 | 14.8 | 14.9 | 15.2 | 15.5 |

## IV. Parameter Identification From Wind Tunnel Tests

Both the static and dynamic test setups are used to identify a complete parameter set for the short period model described in Section II. While the derivatives $C_{m\alpha}$ and $C_{m\eta}$ can be identified from both test campaigns, results from both tests are necessary to obtain a complete model.

### A. Identification From Static Test Data

The static test setup is used to identify $C_{L\alpha}$ and $C_{L\eta}$ as well as $C_{m\alpha}$ and $C_{m\eta}$. For the derivation of $C_{L\alpha}$ and $C_{m\alpha}$, tests are conducted at pitching angles reaching from −20 deg to 20 deg. At each angle of attack, the lift and moment generated by the aircraft are measured, and the corresponding lift coefficient $C_L$ and pitching moment coefficient $C_m$ are calculated. The resulting lift (—●—) and moment (—♦—) coefficients as functions of the angle of attack are shown in the left diagrams of Fig. 4. From the lift coefficient slope, it is apparent that the aircraft shows linear behavior within an angle of attack range of ±10 deg before it reaches stall conditions. Within that range of angle of attacks five test series are conducted to evaluate the aircraft's lift and moment coefficient for an elevator deflection range of ±30 deg. The resulting coefficients from each of those experiments are depicted in the right diagrams of Fig. 4.

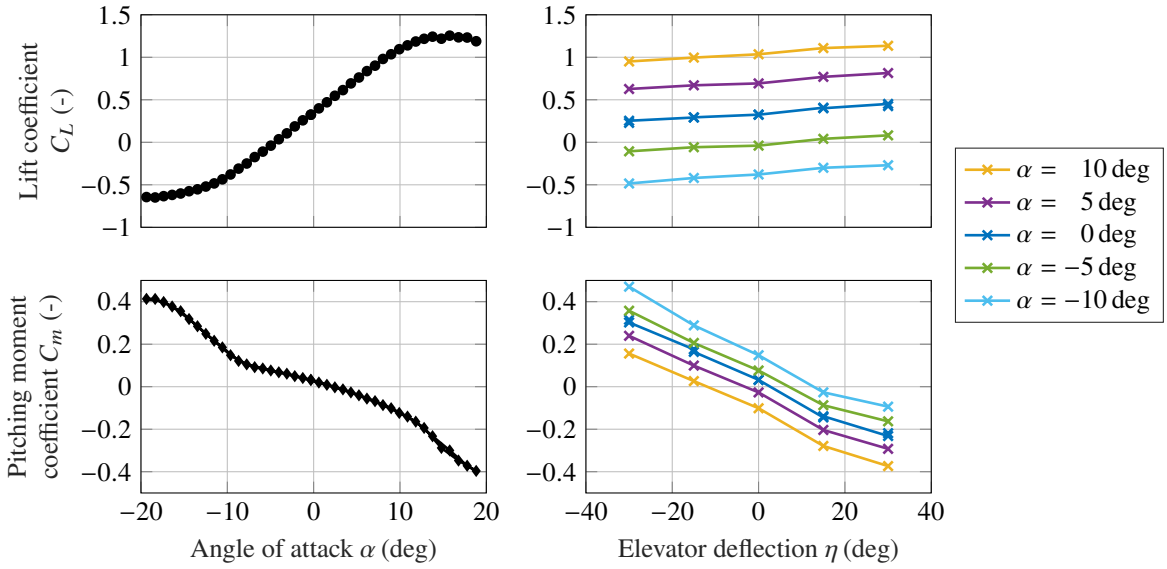


**Fig. 4 Static aerodynamic coefficients for different angles of attacks and different elevator deflections.**

Overall the slopes of the coefficients within the angle of attack range of ±10 deg result in the static parameters listed in Table 3. For conformity, the values in the table are converted to correspond to angular units in radians. While the value for $C_{L\alpha}$, obtained from the static test closely matches the AVL calculation, the static test results for the other parameters deviate from the AVL model by up to 64 %. The greatest deviation is observed in $C_{L\eta}$, which can be attributed to viscous effects that are not covered by the lifting line model used in AVL. Within a thick boundary layer the impact of the elevator deflection on the pressure distribution is reduced. Consequently $C_{m\eta}$ is reduced to a similar extend. In a comparable way, effects of the viscous flow influence the progression of the pitching moment across different angle of attacks. However, in this case the impact of the boundary layer in relation to the overall pitch stiffness $C_{m\alpha}$ is smaller.

**Table 3 Parameter results from static testing**

| | $C_{L\alpha}$ | $C_{L\eta}$ | $C_{m\alpha}$ | $C_{m\eta}$ |
|---|---|---|---|---|
| AVL calculation | 4.60 | 0.05 | −1 | −0.02 |
| Static test result | 4.42 | 0.018 | −0.7 | −0.01 |

### B. Identification from Dynamic Test Data

From the dynamic tests the derivatives $C_{m\alpha}$, $C_{mq}$ and $C_{m\eta}$ are obtained. The parameters are derived from the first chirp input data sets using the *grey box* identification method described in Section II. In this setup, the pitch rate response and elevator input signals are recorded as time series. To ensure the data is suitable for system identification, it is first analyzed and post-processed to minimize effects of measurement noise and test rig vibrations. To evaluate these effects, the frequency content of the output data of the first chirp input test case depicted in Fig. 5, is analyzed across different airspeeds. In all data sets there is a dominant peak in the frequency spectrum outside the excitation profile of the input signal, marked in the diagram with dotted lines. For the measurements at airspeeds between 15 m/s and 17 m/s this peak is located around 3 Hz. In the measurements at airspeeds between 18 m/s and 25 m/s the peak shifts to a frequency of about 4.4 Hz. In all cases the peak is clearly above the frequency range of the excitation signal, indicated in the diagram with a green area. Moreover, it has also been encountered in measurements of test runs without any excitation by the elevator. A deeper analysis revealed that this peak is attributed to the excitation of the six-component ballance on which the aircraft is mounted by the airflow. Although outside of the relevant frequency range for system identification, it is necessary to filter out this effect to avoid any issues arising during the system identification process.

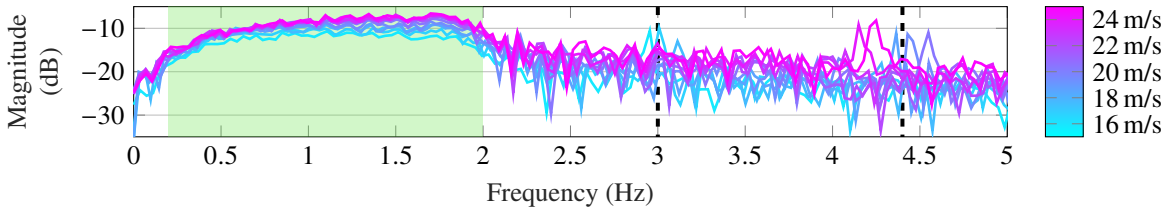


**Fig. 5 Frequency content of the recorded pitch rate data from the identification test case at 15 m/s up to 25 m/s.**

To filter out the vibrations of the ballance from the measured signals, two 5$^{\text{th}}$-order digital butterworth filters are designed. The first filter has a cutoff frequency of 2.5 Hz and is used for the measurements at airspeeds below 18 m/s. The second filter has a corner frequency of 3.5 Hz and is used for the measurements at higher airspeeds. In all scenarios the measurements are processed through the respective filter depending on airspeed before the identification algorithms are applied. Note that the data is processed through the filters both in forward and reverse direction resulting in zero phase distortion.

To furthermore ensure whether the collected pitch rate data is useful for system identification the measurements are analyzed using a coherence spectrum. The coherence spectrum $\kappa_{uy}$ of an input signal $u$ and an output signal $y$ is calculated as

$$\kappa_{uy}(\omega) = \sqrt{\frac{\Phi_{uy}^2(\omega)}{\Phi_{uu}(\omega)\Phi_{yy}(\omega)}} \tag{8}$$

with the cross-correlation spectrum $\Phi_{uy}$ and the auto-correlations $\Phi_{uu}$ and $\Phi_{yy}$ of the signals. The coherence thus varies between 0 and 1 with values close or equal to zero meaning that the behavior of the two signals is uncorrelated [13]. For system identification coherence values close or equal to one are desirable as this means that the behavior of one signal is predictable from the other. Figure 6 shows the coherence of the first chirp signal, which is used in the identification test case with the measured pitch rate for all eleven test conditions. In all performed experiments the coherence values are close to one within the frequency range of the pitching motion. Thus, the content of the measured data, that is attributed to the pitching motion, is sufficiently correlated in all test cases to be used for deriving linear models.

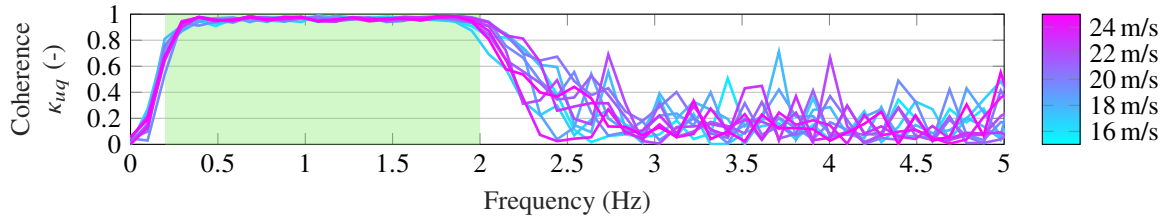


**Fig. 6 Coherence spectras of pitch rate data for the identification chirp case at 15 m/s up to 25 m/s.**

The resulting optimized parameter values for those linear models across all airspeeds are listed in Table 4. Comparing the values resulting for an airspeed of 15 m/s shows, that for $C_{m\alpha}$ and $C_{m\eta}$ the optimized parameters deviate from the initial AVL based estimates in a manner similar to the static test results. This indicates that both tests capture the influence of viscous effects, resulting in a similarly reduced pitch stiffness and elevator pitch moment effectiveness. These findings reinforce confidence in the parameters derived from both tests and validate the dynamic test's ability to accurately identify the actual model parameters. As for $C_{mq}$ which can only be derived from the dynamic test, the optimized parameters are close to the initial AVL based guess of −10.29. This is consistent with the expectation, given that the boundary layer has a smaller effect on dynamic changes in the angle of attack.

**Table 4 Parameter estimation results**

| Airspeed (m/s) | 15 | 16 | 17 | 18 | 19 | 20 | 21 | 22 | 23 | 24 | 25 |
|---|---|---|---|---|---|---|---|---|---|---|---|
| $C_{m\alpha}$ | −0.64 | −0.56 | −0.47 | −0.47 | −0.5 | −0.47 | −0.49 | −0.5 | −0.5 | −0.45 | −0.44 |
| $C_{mq}$ | −14.3 | −13.93 | −10.12 | −9.6 | −10 | −9.01 | −9.32 | −9.39 | −9.47 | −7.67 | −8.47 |
| $C_{m\eta}$ | −0.011 | −0.011 | −0.008 | −0.008 | −0.008 | −0.007 | −0.007 | −0.007 | −0.007 | −0.006 | −0.006 |

To quantify the conformity between the linear models and the measurements, fitness values are derived. The fitness values are calculated as

$$f_y = 100\left(1 - \frac{||y - \hat{y}||_2}{||y - \bar{y}||_2}\right), \tag{9}$$

with the measured outputs $y$ from the experiments, the predicted output $\hat{y}$ from the identified models and the mean of the experimental data $\bar{y}$. The fitness value, derived in percent, is based on the Root Mean Square Error (RMSE) between the measurements $y$ and the predicted output $\hat{y}$ by the model, normalized by the RMSE between the measurements $y$ and their mean value $\bar{y}$. If the model response is equal to the measurements, the RMSE between them is 0, leading to a fitness value of 100 %. A fitness value of 0 % indicates that the RMSE between model and measurements is equal to the RMSE between the measurements and their mean value, i.e., as bad as a constant straight line used as model. Note that the value can fall below 0 % indicating an even worse fit.

The upper diagram in Fig. 7 shows the measured pitch rate from the identification test case at 15 m/s (——) alongside the model response (——) for the pitching motion using AVL-derived parameters as an initial guess. The fitness value in this case is 54 %. The lower diagram illustrated the comparison of the same test case with the calculated response (——) of the model using optimized parameters resulting from the *grey box* identification method described in Section II. With the optimized parameters, the model response fits the measurements significantly better, and the corresponding fitness value improves to 80.8 %.

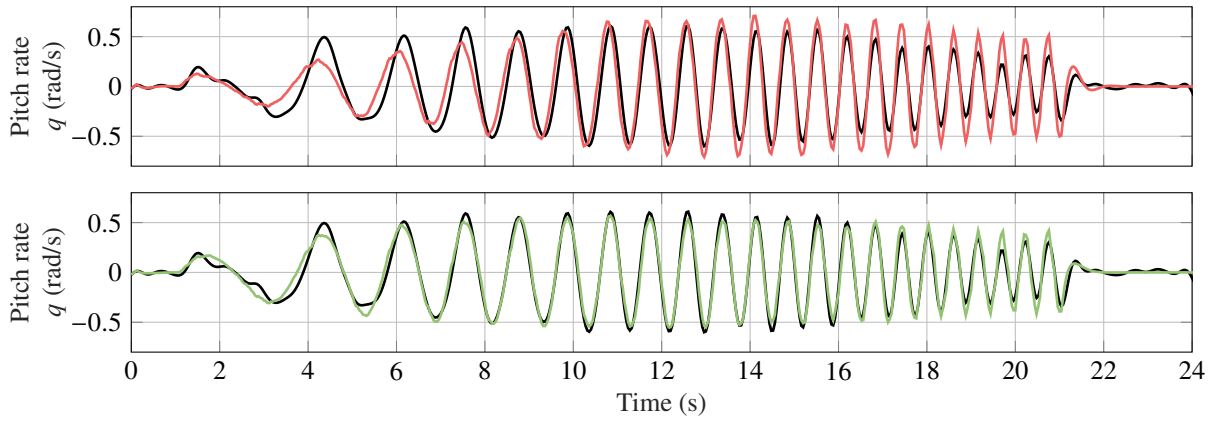


**Fig. 7 Pitch rate comparison between the measurement data (——) against the simulated data from the model with the initial parameter values (——) and the identified parameters values (——) at an airspeed of 15 m/s.**

To ensure that the model dynamics accurately represent the measurements beyond the test case used for the parameter optimization, the resulting models are validated using independent test data. Specifically, the second chirp and the 3211 data sets are used for this validation. In these scenarios, the input signals are applied to the models using the previously determined parameters, and the resulting model responses are compared with the experimental measurements. Figure 8 shows this comparison for both validation cases again at an airspeed of 15 m/s. In the first validation case, shown in the upper diagram, the model is tested using the chirp signal with adapted frequency range. The model response in that case shows very good conformance with the measurements and with a fitness value of 83.9 % demonstrates a performance comparable to the identification case itself. In contrast, the second validation case, using the 3211 signal as elevator deflection input, results in a lower but still acceptable fitness value of 46.2 %. This reduction in fitness is attributed to the lower signal to noise ratio of the 3211 input signal compared to the chirp signal. Still, it is visually observable in the lower diagram of Fig. 8 that the pitch rate response closely follows the experimental measurement data.

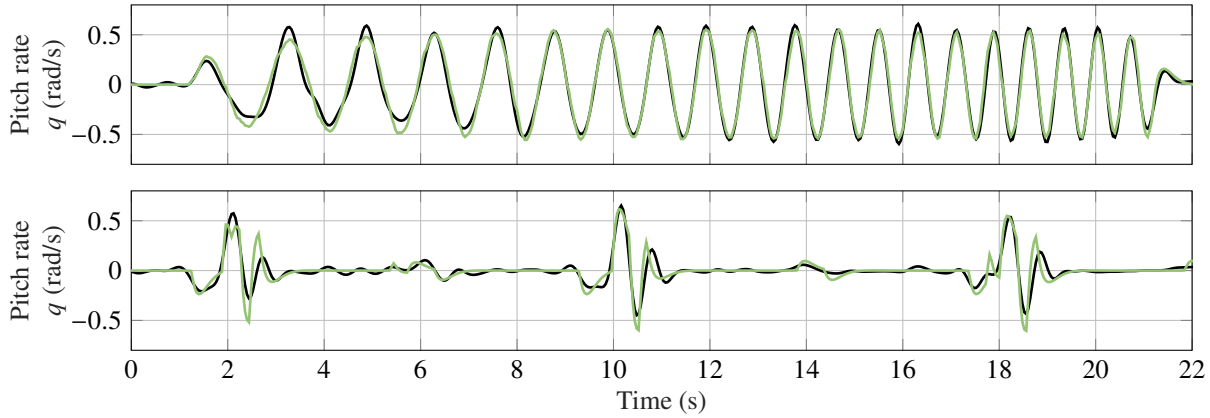


**Fig. 8 Pitch rate comparison between of the identified model data (——) against the measurement data (——) for the two validation test cases at airspeed 15 m/s.**

A summary of the fitness values achieved in both the identification and validation test cases across all airspeeds is presented in Table 5. The fitness values for the identification chirp test case and the validation chirp test case are consistently high, exceeding 80 %, indicating strong agreement between the model and experimental measurements. Similarly, the fitness values for the 3211 validation test case are generally high, despite the lower signal to noise ratio of this input signal. The lowest fitness value occurs for the 3211 test case at an airspeed of 15 m/s that is shown in Fig. 8. However, for all other airspeeds, the fitness values in the 3211 test cases exceed 50 %, reaching up to 68 %. Overall this confirms that the resulting models with the optimized parameters accurately represent the actual pitching dynamics of the aircraft in the test rig.

**Table 5 Fitness values for the identification and the validation test scenarios from the dynamic tests**

| Airspeed (m/s) | 15 | 16 | 17 | 18 | 19 | 20 | 21 | 22 | 23 | 24 | 25 |
|---|---|---|---|---|---|---|---|---|---|---|---|
| Identification chirp fitness values (%) | 80.8 | 81.9 | 82.8 | 84.7 | 83.2 | 84.9 | 84.7 | 85.1 | 84.8 | 84.4 | 84.8 |
| Validation chirp fitness values (%) | 83.9 | 81.7 | 82.4 | 83.2 | 85.3 | 83.8 | 85.2 | 84.6 | 85.7 | 82.9 | 83.2 |
| Validation 3211 fitness values (%) | 46.2 | 52.8 | 58.6 | 65.2 | 63.1 | 60.9 | 68.2 | 54.1 | 51.5 | 61.6 | 55.3 |

### C. Short Period Model Results

The complete short period model is constructed using $C_{L\alpha}$ and $C_{L\eta}$ derived from the static tests, along with $C_{m\alpha}$ $C_{mq}$ and $C_{m\eta}$ at each airspeed obtained from the dynamic tests. The natural frequency and damping ratio $\zeta$ of the resulting models are calculated and compared across the entire airspeed range, as shown in Fig. 9. The right diagram demonstrates, that the models have consistently high damping values of approximately 0.8 across the airspeed range, indicating well-damped short period motion. The left diagram shows the natural frequency $\omega_n$ of the short period model

at the aircraft's cruise speed of 17 m/s to be approximately 1.8 Hz. This value closely aligns with the initial estimate of 1.5 Hz based on the AVL calculation. The natural frequency increases with airspeed, reflecting behavior consistent with realistic short period dynamics. Overall, the resulting values and their trends across the airspeed range reinforce confidence that the models, built using parameters derived from the static and dynamic tests, accurately represent the aircraft's actual short period dynamics.

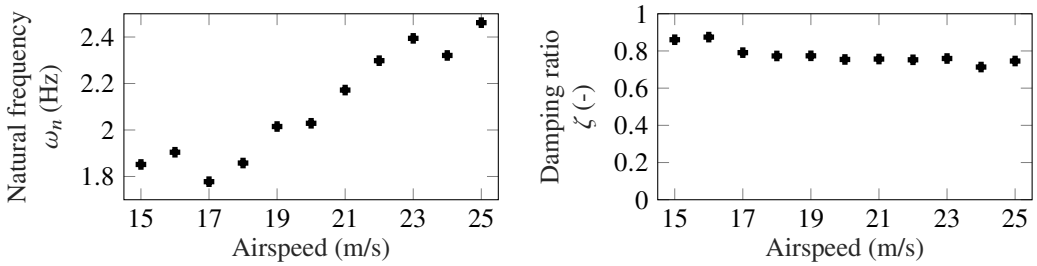


**Fig. 9 Natural frequency and damping ratio of the short period models across the investigated airspeed range.**

## V. Conclusion

A test campaign with a combination of static and dynamic wind tunnel testing techniques was performed for a small fixed-wing UAS to obtain short period models across an airspeed range of 15 to 25 m/s. In the static setup, the test rig's traverse system and a six-component balance were used to measure the aircraft's lift and pitch moment under various angle of attack and elevator deflection configurations. The time averaged measurements from these tests are used to directly derive the aircraft's static aerodynamic derivatives $C_{L\alpha}$, $C_{L\eta}$, $C_{m\alpha}$ and $C_{m\eta}$. In the dynamic setup, the aircraft's pitching dynamics were excited using two different chirp signals and a 3211 elevator deflection signal across the investigated airspeed range. From the gathered data $C_{m\alpha}$, $C_{mq}$ and $C_{m\eta}$ are derived using a *grey box* approach. The parameters obtained from both experiments were combined to construct short period models for the investigated UAV. Analyses of the natural frequency and damping ratio of the resulting models demonstrated behavior consistent with realistic short period dynamics.

## Acknowledgments

This research was funded by the German Federal Ministry for Digital and Transport under grant number 19F1176A entitled "Energieeffiziente, datengetriebene UAS Trajektorienplanung unter Berücksichtigung makro- und mikrometeorologischer Randbedingung – EndeAR". The responsibility for the content of this paper is with its authors. The financial support is gratefully acknowledged.

## References

[1] Simmons, B. M., Gresham, J. L., and Woolsey, C. A., "Flight-Test System Identification Techniques and Applications for Small, Low-Cost, Fixed-Wing Aircraft," *Journal of Aircraft*, Vol. 60, No. 5, 2023, pp. 1503–1521. doi:10.2514/1.C037260.

[2] Pfifer, H., and Danowsky, B. P., "System Identification of a Small Flexible Aircraft - Invited," *AIAA Atmospheric Flight Mechanics Conference*, American Institute of Aeronautics and Astronautics, San Diego, California, USA, 2016. doi:10.2514/6.2016-1750.

[3] Jategaonkar, R. V., *Flight Vehicle System Identification: A Time Domain Methodology*, American Institute of Aeronautics and Astronautics, Reston ,VA, 2006. doi:10.2514/4.866852.

[4] Hoffer, N. V., Coopmans, C., Jensen, A. M., and Chen, Y., "A Survey and Categorization of Small Low-Cost Unmanned Aerial Vehicle System Identification," *Journal of Intelligent & Robotic Systems*, Vol. 74, No. 1-2, 2014, pp. 129–145. doi:10.1007/s10846-013-9931-6.

[5] Magill, J. C., Cataldi, P., Morency, J. R., Hammer, D. X., Burgess, R., and Jeter, E., "Demonstration of a Wire Suspension for Wind-Tunnel Virtual Flight Testing," *Journal of Spacecraft and Rockets*, Vol. 46, No. 3, 2009, pp. 624–633. doi:10.2514/1.39188.

[6] Ignatyev, D. I., Sidoryuk, M. E., Kolinko, K. A., and Khrabrov, A. N., "Dynamic Rig for Validation of Control Algorithms at High Angles of Attack," *Journal of Aircraft*, Vol. 54, No. 5, 2017, pp. 1760–1771. doi:10.2514/1.C034167.

[7] Li, H., Li, Y., Zhao, Z., Wang, X., Yang, H., and Ma, S., "High-Speed Virtual Flight Testing Platform for Performance Evaluation of Pitch Maneuvers," *Aerospace*, Vol. 10, No. 11, 2023, p. 962. doi:10.3390/aerospace10110962.

[8] Araujo-Estrada, S. A., Lowenberg, M. H., and Neild, S. A., "Capturing Nonlinear Time-Dependent Aircraft Dynamics Using a Wind Tunnel Manoeuvre Rig," *Aerospace Science and Technology*, Vol. 121, 2022, p. 107325. doi:10.1016/j.ast.2021.107325.

[9] O'Donnell, R. S., and Mohseni, K., "Aerodynamic Parameter Estimation from Wind Tunnel Testing of a Small UAS," *2018 AIAA Atmospheric Flight Mechanics Conference*, American Institute of Aeronautics and Astronautics, Kissimmee, Florida, 2018. doi:10.2514/6.2018-0294.

[10] Orlik-Ruckemann, K., "Review of techniques for determination of dynamic stability parameters in wind tunnels," *AGARD Lecture Series*, , No. 114, 1981.

[11] Bergmann, A., "Modern Wind Tunnel Techniques for Unsteady Testing – Development of Dynamic Test Rigs," *Hermann Schlichting – 100 Years*, Vol. 102, edited by R. Radespiel, C.-C. Rossow, and B. W. Brinkmann, Springer Berlin Heidelberg, Berlin, Heidelberg, 2009, pp. 59–77. doi:10.1007/978-3-540-95998-4_5.

[12] Keesman, K. J., *System Identification: An Introduction*, Advanced Textbooks in Control and Signal Processing, Springer London, London, 2011. doi:10.1007/978-0-85729-522-4.

[13] Ljung, L., *System Identification: Theory for the User*, 2nd ed., Prentice Hall Information and System Sciences Series, Prentice Hall PTR, Upper Saddle River, NJ, 1999.

[14] Drela, M., and Youngren, H., *Athena Vortex Lattice 3.36*, Massachusetts Institute of Technology, 2017.